Scientific Research Publishing

Advances in Materials Physics and Chemistry, 2023, 13, 207-217
https://www.scirp.org/journal/ampc
ISSN Online: 2162-5328
ISSN Print: 2162-531X

Performance Analysis of a Radial N^+/P Silicon Solar Cell in Steady State and Monochromatic Illumination

Aboubacar Savadogo, Bernard Zouma, Bruno Korgo, Ramatou Konaté, Sie Kam

Departement de Physique, Laboratoire d'Energies Thermiques Renouvelables, Unité de Formation et de Recherche en Sciences exactes et appliquées, Université Joseph KI-ZERBO, Ouagadougou, Burkina Faso
Email: bernard_zoum@ujkz.bf

How to cite this paper: Savadogo, A., Zouma, B., Korgo, B., Konaté, R. and Kam, S. (2023) Performance Analysis of a Radial N^+/P Silicon Solar Cell in Steady State and Monochromatic Illumination. *Advances in Materials Physics and Chemistry*, **13**, 207-217.
https://doi.org/10.4236/ampc.2023.1312015

Received: November 21, 2023
Accepted: December 25, 2023
Published: December 28, 2023

Abstract

In this paper, we investigate theoretically a radial n^+/p silicon solar cell in steady state and monochromatic illumination. The purpose of this work is to analyze the effect of the cell base radius on its electrical parameters. The continuity equation in cylindrical coordinates is established and solved based on Bessel functions and boundaries conditions; this led us to the photovoltage and photocurrent density in the cell. The open circuit voltage and the short circuit current density are then deduced and analyzed considering the base radius. Based on J-V and P-V curves, series and shunt resistances, fill factor and maximum power point are derived and the conversion efficiency of the cell is deduced. We showed that short circuit current density, maximum power, conversion efficiency and shunt resistance decrease with increasing base radius contrary to the open circuit voltage, the fill factor and the series resistance.

Keywords

Solar Cell, Radial Junction, Shunt and Series Resistances, Conversion Efficiency

1. Introduction

To improve the performance and reduce the cost of solar cells or to overcome the limitations exhibited by Shockley and Queisser [1], many and diverse studies on n-p junction solar cells are conducted. There are thus several configurations: we encounter parallelepiped or cubic configuration with the classic horizontal junction between the base and emitter assuming that the generated carriers

move from the base to the emitter parallel to the illumination [2] [3] [4] and vertical junction for the purpose to reduce the path of the carriers to the junction to decrease recombination in the base of the cell [5] [6] [7]. Also, we can find in the literature cylindrical configurations with planar [8] [9] [10] and radial [11] [12] [13] [14] p-n junction as depicted in **Figure 1** which is deeply investigated in this paper.

Trabelsi *et al.* [9] and Mbodji *et al.* [8] carried out work on a cylindrical grain N^+/P polycrystalline solar cell. The study [9] reveals that the recombination at the grain boundaries becomes non-negligible and the photocurrent decreases for a photovoltaic cell whose thickness H is greater than the diffusion length for a small cylindrical grain radius. And the optimum thickness to obtain more than 95% of the available current density is around 50 μm. And on the other hand Mbodji *et al.* [9] showed that photocurrent density and photovoltage increase with grain radius. And the shunt resistance also increases with the radius of the grain for large values of the dynamic speed at the junction.

Leye *et al.* [10] studied the temperature effect on the performance of an N/P solar cell considering the columnar cylindrical grain. They showed that when the temperature increases the short circuit increases however, the open circuit decreases. Some parameters, such as the short-circuit photocurrent density, the open circuit photovoltage, the fill factor, and the efficiency are linearly dependent on the temperature. These results mentioned above were obtained by considering a planar junction.

As for the radial junction, it should be noted that it is essentially perceived in nanotechnologies such as nanowires offering many advantages. Failing to increase the maximum efficiency beyond the standard limits, radial geometry allows to reduce both the quantity and quality of the material necessary to approach these limits, thus allowing a substantial reduction in costs [12] [13].

The geometric configuration of solar cells therefore seems to be a key element. Especially since studies carried out on cubic and cylindrical solar cells have shown a slight improvement in photovoltaic performance in favor of the cylindrical model [9]. Simulation work has highlighted the advantage of the radial junction over a planar junction [14].

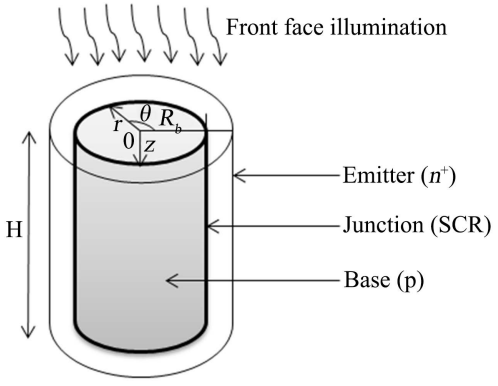

Figure 1. Radial p-n junction solar cell.

Sam *et al.* [11] were able, through a 2D approach, to study the effect of the base radius, the thickness and the wavelength on the photocurrent density and the quantum efficiency of a radial junction solar cell. However their study doesn't give any information on the effect of the base radius on the other electrical parameters such as photovoltage, electric power, fill factor, shunt and series resistances.

The purpose of this article is to broaden the field of study in this field by studying the influence of the base radius of a radial junction cell on its electrical parameters.

2. Theoretical Background

Our model is illustrated in **Figure 1**. It consists of three parts including two coaxial cylinders:

- The first solid cylinder forms the base of the solar cell. It is a p-type region (10^{15} to 10^{17} cm^{-3}) of radius R_b and depth H with the predominance of generation, recombination and diffusion phenomena.
- The second hollow cylinder, which circles the first one, represents the n^+-type emitter of thickness d and is heavily doped (10^{18} to 10^{19} cm^{-3}).
- The third part is what is called the space charge region (SCR). Located and created between the emitter and the base, it is a transition region where there is an intense electric field which separates electron-hole pairs arriving at the junction.

2.1. Assumptions

To simplify our study, we assume that:

- The contribution of the emitter is not considered [8] [11] also implying the non-taking into account of the grain limits.
- The penetration of light is along the z- axis parallel to the junction and the generation of excess minority charge carriers.
- The transport of excess minority charge carriers is according to the position r in the base [14].
- The base doping is uniform, so no field exists outside the space charge regions: the base is quasi-neutral [9] [15].
- The Earth's magnetic field is not considered because that magnetic fields of values smaller than 10^{-5} T have no significant effect on a solar cell [2].

2.2. Continuity Equation

When the solar cell is illuminated, there are three major phenomena that occur inside: carrier generation, recombination, and drift/diffusion. These phenomena are described by the continuity equation. Assuming that carriers generation is uniform according to θ and taking into account the symmetry of the model, carriers density should be invariant by any θ angle rotation [8] [10] [13] [16]. The continuity equation can then be written as:

$$\frac{\partial^2 \delta_n(r,z,\lambda)}{\partial r^2}+\frac{1}{r}\cdot\frac{\partial \delta_n(r,z,\lambda)}{\partial r}+\frac{\partial^2 \delta_n(r,z,\lambda)}{\partial z^2}-\frac{\delta_n(r,z,\lambda)}{L_n^2}=-\frac{\alpha(\lambda)(1-R)\phi_0 e^{-\alpha(\lambda)z}}{D_n} \quad (1)$$

δ_n is the excess minority carrier density, λ the illumination wavelength, α the absorption coefficient, R the reflection coefficient, ϕ_0 the incident flux, L_n the excess minority carrier diffusion length and D_n their diffusion constant in the base of the cell. r and z represent respectively the radius and thickness of the base along horizontal and vertical axes.

Equation (1) is a partial differential equation whose general solution can be given in the following form [9] [11]:

$$\delta_n(r,z,\lambda)=\sum_{k\geq 0} f(r,\lambda)\sin(C_k z) \quad (2)$$

C_k and $f(r, \lambda)$ are obtained from the following boundaries conditions:

- At the emitter base interface ($r = R_b$):

$$\left.\frac{\partial \delta_n(r,z,\lambda)}{\partial r}\right|_{r=R_b}=-\frac{S_f}{2D_n}\cdot\delta_n(R_b,z,\lambda) \quad (3)$$

- At the backside ($z = H$):

$$\left.\frac{\partial \delta_n(r,z,\lambda)}{\partial z}\right|_{z=H}=-\frac{S_b}{D_n}\cdot\delta_n(r,H,\lambda) \quad (4)$$

With S_f and S_b respectively the junction dynamic velocity and the back surface recombination velocity.

- At the front side ($z = 0$):

$$\delta_n(r,z=0,\lambda)=0 \quad (5)$$

3. Electrical Parameters

3.1. Photocurrent Density

The photocurrent density is determined by using Fick's law:

$$J_{ph}=\frac{qD_n}{\pi R_b^2}\int_0^H \left.\frac{-\partial \delta_n(r,z,\lambda)}{\partial r}\right|_{r=R_b}(2\pi R_b)\,dz \quad (6)$$

q is the electron charge.

Inserting Equation (3) into Equation (6) and doing the integration, we obtain Equation (7):

$$J_{ph}=\sum_{k\geq 0}\frac{-qS_f}{R_b C_k}\left[A_k(\lambda)I_0\left(\frac{R_b}{L_{nk}}\right)+M_k(\lambda)\right]\left[\cos(C_k H)-1\right] \quad (7)$$

In Equation (7) I_0 represent the Bessel function of modified 1st species of order 0, the expressions of M_k and A_k are given by Equations (8) and (9) respectively

$$M_k(\lambda)=\frac{2\alpha(\lambda)(1-R(\lambda))\phi_0 L_{nk}^2 C_k^2\left[1+(-1)^{k+1}\exp(-\alpha H)\right]}{D_n\left(C_k^2+\alpha^2\right)\left(C_k H-\sin(C_k H)\cos(C_k H)\right)} \quad (8)$$

$$A_k(\lambda) = -\frac{M_k(\lambda)}{\frac{2D_n}{S_f L_{nk}} I_0'\left(\frac{R_b}{L_{nk}}\right) + I_0\left(\frac{R_b}{L_{nk}}\right)} \tag{9}$$

3.2. Photovoltage

The photovoltage is obtained from Boltzmann relation in the form:

$$V_{ph} = V_T \ln\left[1 + \frac{1}{n_0}\int_0^H \delta_n\left(r = R_b, z, \lambda\right)\left(2\pi R_b\right)\mathrm{d}z\right] \tag{10}$$

By using Equation (3), Equation (10) can be rewritten as:

$$V_{ph} = V_T \ln\left[1 + \frac{4\pi R_b D_n}{n_0 S_f}\sum_{k\geq 0}\frac{A_k(\lambda) I_0'\left(\frac{R_b}{L_{nk}}\right)}{C_k L_{nk}}\left[\cos\left(C_k H\right) - 1\right]\right] \tag{11}$$

$V_T = \frac{K_B T}{q}$ is the thermal voltage, $n_0 = \frac{n_i^2}{N_B}$ is the electron density at equilibrium, n_i the intrinsic carrier's density, N_B the base doping density and K_B the Boltzmann constant.

4. Results and Discussion

Figure 2 presents the photocurrent density versus junction dynamic velocity for various base radius.

For lower S_f ($\leq 10^2$ cm/s) the photocurrent is practically zero; carriers' flow through the junction is very low: there are charge accumulations about the junction. The solar cell is operating in open circuit. After an intermediate operation, we observe that when S_f becomes very important ($S_f \geq 10^6$ cm/s), the photocurrent density is maximum. Carriers' flow through the junction is very high: this is a short-circuit situation. This result is in good agreement with those already obtained in other works, both with the radial junction [11] and with the planar junction [8]. The decrease in the photocurrent density J_{ph} observed with the increase of the base radius R_b is explained by the fact that when R_b increases the n-p junction becomes more distant. Carriers generated close to the center that is far from the junction are subject of recombination. Only those generated far from the center and close to the junction according to the diffusion length L_n will be able to participate in the photocurrent.

In Figure 3, we plotted the photovoltage versus junction dynamic velocity for various base radius.

As noted on Figure 3, when the cell radius increases there is more carrier's accumulation across the junction. The more the cell radius is, the more the n-p junction is far for charge carrier. For those carriers not recombined, there is an accumulation and then an increase of the photovoltage.

Those observations can be seen on Figure 4 with the Photocurrent density versus Photovoltage curves.

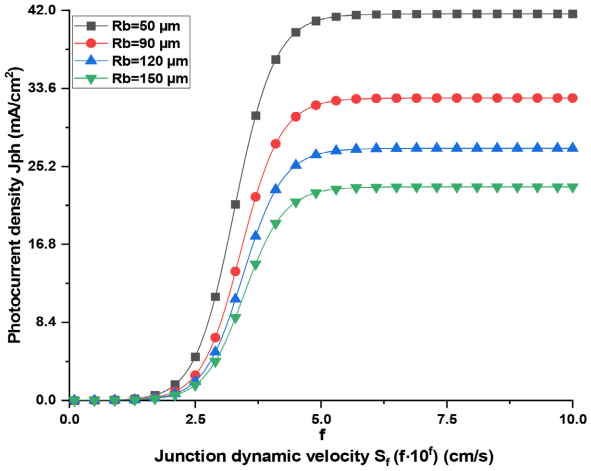

Figure 2. Photocurrent density versus junction dynamic velocity for various base's radius. L_n = 50 µm, H = 150 µm, $S_b = 2 \times 10^2$ cm/s, λ = 1000 nm.

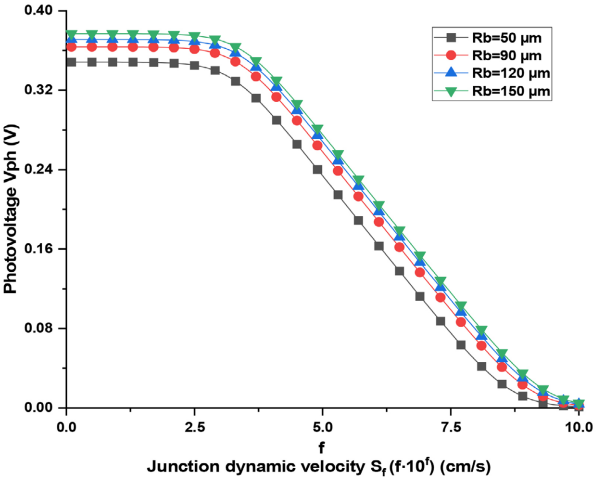

Figure 3. Photovoltage versus junction dynamic velocity for various base's radius. L_n = 50 µm, λ = 1000 nm, H = 150 µm, $S_b = 2 \times 10^2$ cm/s.

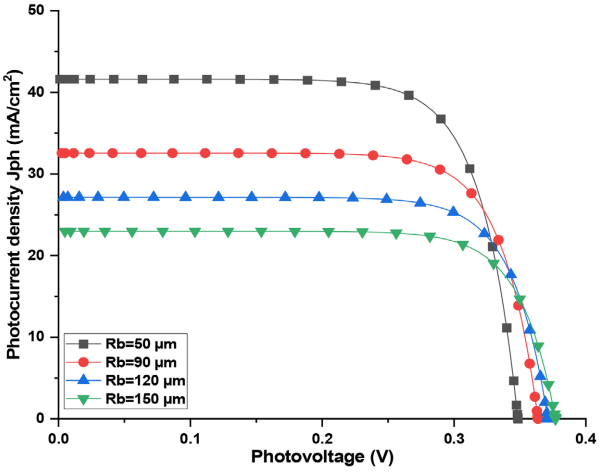

Figure 4. Photocurrent density versus photovoltage for various base's radius. $S_b = 2 \times 10^2$ cm/s, H = 150 µm, λ = 1000 nm, L_n = 50 µm.

The short circuit current density decreases with increasing base radius while the open circuit voltage increases. Figure 4 also shows that short circuit current density is more sensitive to the base radius contrary to the open circuit voltage.

For a given Photocurrent density—Photovoltage curve, the solar cell behaves like a real current generator near short circuit and like a real voltage generator near open circuit. The solar cell can then be represented by the following electrical equivalent circuits [6] [7].

From the electrical equivalent circuits depicted in Figure 5 and Figure 6, expressions of shunt and series resistances are derived as follow:

$$R_s = \frac{V_{phco} - V_{ph}\left(S_f\right)}{J_{ph}\left(S_f\right)} \tag{12}$$

$$R_{sh} = \frac{V_{ph}\left(S_f\right)}{J_{phcc} - J_{ph}\left(S_f\right)} \tag{13}$$

Series and shunt resistances curves are presented respectively on Figure 7 and Figure 8 versus junction dynamic velocity for various base radiuses.

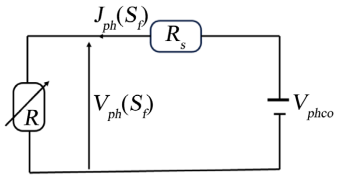

Figure 5. Solar cell electrical equivalent circuit near open circuit.

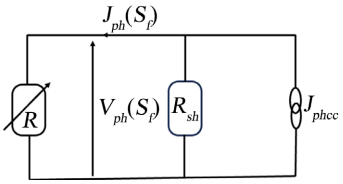

Figure 6. Solar cell electrical equivalent circuit near short circuit.

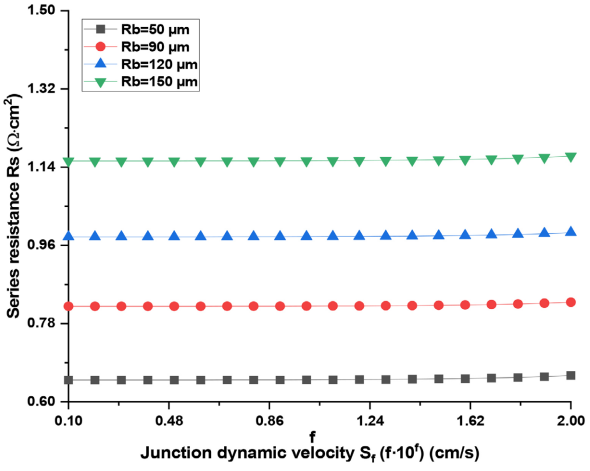

Figure 7. Series resistance versus junction dynamic velocity for various base's radius. S_b = 2×10^2 cm/s, H = 150 µm, L_n = 50 µm, λ = 1000 nm.

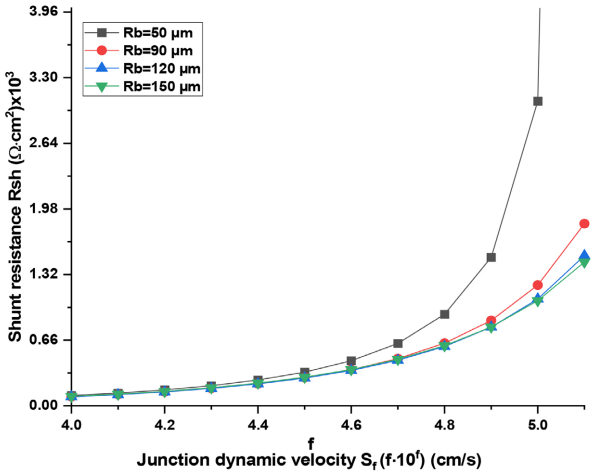

Figure 8. Shunt resistance versus junction dynamic velocity for various base's radius R_b; $S_b = 2 \times 10^2$ cm/s, $H = 150$ µm, $L_n = 150$ µm, $\lambda = 1000$ nm.

Beyond a slight increase in the series resistance R_s with increasing junction dynamic velocity, it can be noticed through **Figure 7**, that when R_b increases the series resistance increases. This result is consistent with those observed above with the photocurrent density. There is a decrease in J_{ph} with R_b which is explained by a loss of carriers in the base of the cell and an inability of these carriers to be able to cross the junction to participate in the photocurrent. Then the photocurrent transmitted to the external load decreases, thus suggesting an increase in the series resistance which shows a multiplication of the defects of the material or even of the cell through the increase in the radius R_b.

Also, it is noted through **Figure 8** that the shunt resistance (R_{sh}) increases as the dynamic velocity at the S_f junction increases. Indeed, when S_f increases more carriers manage to cross the junction to participate in the photocurrent. Thus, fewer carriers are recombined. The current transmitted to the external load is improved. Then the leakage currents are reduced which reflects the increase in shunt resistance. However, when the base radius R_b increases the shunt resistance R_{sh} decreases. This is the consequence of the decrease in the photocurrent density and the increase in the open circuit photovoltage with increasing base radius (**Figure 2** and **Figure 3**). The current transmitted to the external load is reduced through the increase in leakage currents, which partly explains the decrease in the shunt resistance R_{sh}.

Figure 9 presents the output power versus photovoltage for various base's radius Rb.

The output power increases with the photovoltage up to a maximum value, called the maximum power point or peak power, before decreasing and canceling out at the open circuit. Increasing the radius of the base leads to a decrease in maximum power (P_m) and an increase in circuit voltage (V_{oc}). Moreover, we noticed that the more R_b increases, the more the maximum power point is shifted right. That is, the increase in R_b leads to an increase of the fill factor (FF) and contributes to reduce the efficiency (η) of the cell as can be seen with **Table 1**.

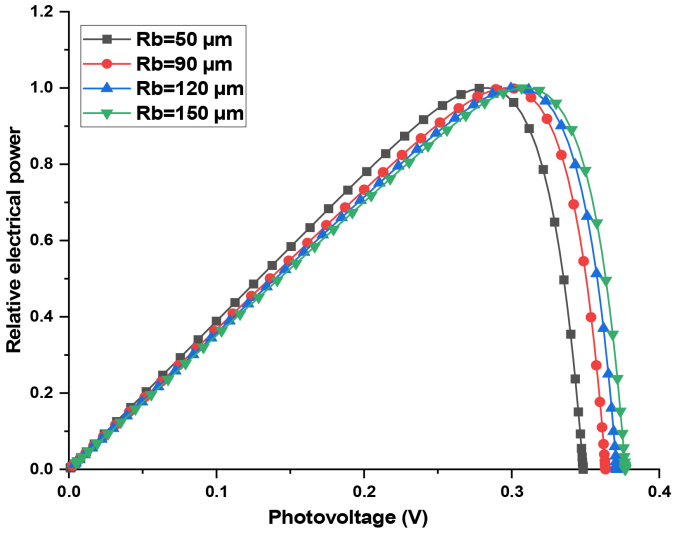

Figure 9. Output power versus photovoltage for various base's radius R_b. $S_b = 2 \times 10^2$ cm/s, $H = 150$ µm, $\lambda = 1000$ nm, $L_n = 50$ µm.

Table 1. Electrical parameters of the solar cell for various base radius.

R_b (µm)	20	40	50	90	120	150
$J_{ph\max}$ (mA/cm^2)	43.122	40.297	37.694	30.028	24.845	21.375
$V_{ph\max}$ (mV)	259.81	274.2	284.07	295.54	305.57	306.7
$P_{\max}$ (mW/cm^2)	11.204	11.05	10.708	8.874	7.591	6.555
J_{cc} (mA/cm^2)	48.128	43.961	41.616	32.652	27.144	22.996
V_{oc} (mV)	324.56	342.58	348.38	363.67	371.15	376.95
FF (%)	71.72	73.37	73.85	74.93	75.34	75.61
η (%)	22.408	22.10	21.416	17.748	15.182	13.11

5. Conclusion

In this paper, we studied the effect of the base radius on the electrical parameters of a radial n-p junction solar cell. After establishing and solving the continuity equation in cylindrical coordinates, new expressions for the photovoltage and the photocurrent density were deduced. This allowed the deduction of the series and shunt resistances, the fill factor (FF) and conversion efficiency. The study reveals that when the radius of the base increases, the short-circuit current density, the maximum power, shunt resistance and the conversion efficiency (η) decrease. However, there is an increase in the open circuit photovoltage, the fill factor and the series resistance.

Acknowledgment

The authors wish to express their gratitude to the international Scientific Program (ISP), University of Uppsala, Sweden for financial support through the

project BUF01.

Conflicts of Interest

The authors declare no conflicts of interest regarding the publication of this paper.

References

[1] Shockley, W. and Queisser, H.J. (1961) Detailed Balance Limit of Efficiency of *p-n* Junction Solar Cells. *Journal of Applied Physics*, **32**, 510-519. https://doi.org/10.1063/1.1736034

[2] Zouma, B., Maiga, A., Dieng, M., Zougmore, F. and Sissoko, G. (2009) 3d Approach of Spectral Response for A Bifacial Silicon Solar Cell under A Constant Magnetic Field. *Global Journal of Pure and Applied Sciences*, **15**, 117-124. https://doi.org/10.4314/gjpas.v15i1.44908

[3] Zoungrana, M., Zerbo, I., Sere, A., Zouma, B. and Zougmore, F. (2011) 3D Study of Bifacial Silicon Solar Cell under Intense Light Concentration and under External Constant Magnetic Field. *Global Journal of Engineering Research*, **10**, 113-124.

[4] Sourabié, I., *et al.* (2022) Three-Dimensional Study of the Effect of the Angle of Incidence of a Magnetic Field on the Electrical Power and Conversion Efficiency of a Polycrystalline Silicon Solar Cell under Multispectral Illumination. *Smart Grid Renew. Energy*, **13**, 295-304. https://doi.org/10.4236/sgre.2022.1312018

[5] Wise, J.F. (1970) Vertical Junction Hardened Solar Cell. US Patent No. 3690953A.

[6] Ibra, N.M., *et al.* (2012) Theoretical Study of a Parallel Vertical Multijunction Silicon Cell under Multispectral Illumination: Influence of External Magnetic Field on the Electrical Parameters. *International Journal of Advanced Technology & Engineering Research*, **2**, 101-109.

[7] Mballo, O., Seibou, B., Wade, M., Diouf, M.S. and Ly, I. (2016) Influence of the Depth Base on the Electrical Parameters of a Parallel Vertical Junction Silicon Solar Cell under Polychromatic illumination. *International Journal of Electrical Engineering*, **4**, 6-16.

[8] Diouf, A., Diao, A. and Mbodji, S. (2018) Effect of the Grain Radius on the Electrical Parameters of an N^+/P Polycrystalline Silicon Solar Cell under Monochromatic Illumination Considering the Cylindrical Orientation. *Journal of Scientific and Engineering Research*, **5**, 174-180.

[9] Trabelsi, A., Zouari, A. and Ben Arab, A. (2009) Modeling of Polycrystalline N^+/P Junction Solar Cell with Columnar Cylindrical Grain. *Revue des Energies Renouvelables*, **12**, 279-297. https://doi.org/10.54966/jreen.v12i2.139

[10] Leye, S.N., Fall, I., Mbodji, S., Sow, P.L.T. and Sissoko, G. (2018) Analysis of T-Coefficients Using the Columnar Cylindrical Orientation of Solar Cell Grain. *Smart Grid and Renewable Energy*, **9**, 43-56. https://doi.org/10.4236/sgre.2018.93004

[11] Sam, R., Diasso, A., Zouma, B. and Zougmoré, F. (2020) 2D Modeling of Solar Cell *p-n* Radial Junction: Study of Photocurrent Density and Quantum Efficiency in Static Mode under Monochromatic Illumination. *Smart Grid and Renewable Energy*, **11**, 191-200. https://doi.org/10.4236/sgre.2020.1112012

[12] Garnett, E.C., Brongersma, M.L., Cui, Y. and McGehee, M.D. (2011) Nanowire Solar Cells. *Annual Review of Materials Research*, **41**, 269-295. https://doi.org/10.1146/annurev-matsci-062910-100434

https://www.annualreviews.org/doi/10.1146/annurev-matsci-062910-100434

[13] Gharghi, M. (2012) On the Design and Applicability of Nanowire Solar Cells Using Low-Grade Semiconductors. *Journal of Applied Physics*, **111**, Article ID: 034501. https://doi.org/10.1063/1.3679134

[14] Kayes, B.M., Atwater, H.A. and Lewis, N.S. (2005) Comparison of the Device Physics Principles of Planar and Radial *p-n* Junction Nanorod Solar Cells. *Journal of Applied Physics*, **97**, Article ID: 114302. https://doi.org/10.1063/1.1901835

[15] Zerbo, I., Zoungrana, M., Sourabié, I., Ouedraogo, A., Zouma, B. and Bathiebo, D.J. (2016) External Magnetic Field Effect on Bifacial Silicon Solar Cell's Electrical Parameters. *Energy and Power Engineering*, **8**, 146-151. https://doi.org/10.4236/epe.2016.83013

[16] Elnahwy, S. and Adeeb, N. (1988) Exact Analysis of a Three-Dimensional Cylindrical Model for a Polycrystalline Solar cell. *Journal of Applied Physics*, **64**, 5214-5219. https://doi.org/10.1063/1.342435